ISSN:2790-1688 Volume-15-(2025)

The Enhanced Oxygen Evolution Reaction Electrocatalytic Performance of Zr-Substituted nano-CeO2 with Algorithm-Assisted Optimization

Roy Lu

Shanghai SMIC Private School,Shanghai,201203,China

Abstract. Immediate research is needed on the possibility of developing noble-metal-free oxygen evolution reaction (OER) based electrocatalysts to develop sustainable, economical water-splitting technology. Improvement of rare-earth oxide and transition metal catalysts by compositional and process modifications is considered to be quite challenging due to the challenge of a perfect combination of properties with dopant concentration and amount of precursors deposited under certain thermal treatment conditions. This paper reports on the electrocatalytic characteristics of the thin-film electrodes that are fabricated using Zr-doped cerium oxide at varying concentrations of Zr, 1-5 per cent by mass. Electrochemical characterisation was done using linear sweep voltammetry (LSV), Tafel slope analysis, electrochemical impedance spectroscopy (EIS), and the stability test of all compositions. The controlled machine learning (ML) model using gradient boosting regression (GBR) was provided with experimentally determined overpotential values as training data in order to obtain a reasonable setting in a minimum amount of time. The ML model displayed a fast prediction speed and gave insight into how 3 mass%Zr doping leads to the best OER activity. The electrode optimised by doping 3mass%Zr in the CeO_2 revealed a low onset potential of 1.39 V against RHE, an overpotential of 319 mV at 10 mA/cm2, and a low Tafel slope of 85.7 mV dec 1, which exceeds that of the other compositions. The composition exhibited long-term stability in operation, having retained 84 per cent of its initial current density after 48 hours of continuous testing, thus presenting enhanced mass activity. The findings illustrate the synthetic influence of Zr on the electronic divide and the surface picture of the CeO_2, showing the eminence of the procedure of info-driven design as a strategy that can be used to discover catalysts. With the guidance of ML, the framework has the potential to assist the researchers in devising a universal algorithm that can be used to develop high-performance OER electrocatalysts based on non-precious metals in the future.

Keywords: Zr-doped CeO_2;Oxygen evolution reaction (OER); Machine learning optimization.

1. Introduction

The continued use of fossil fuels has contributed to the rapid depletion of non-renewable sources of energy, together with severely damaging environmental factors due to the imminent production of greenhouse gases and massive pollution.[1, 2] The scientific community is currently dwelling on the mass production of sustainable energy sources that are friendly to the environment. The scientific fraternity has recognised hydrogen as a potential carrier of clean energy due to the fact that it possesses high energy density and zero-emission combustion capability, and various opportunities of application, such as in transportation or chemical manufacturing. Hassan et al. The researchers in the study assessed the advantages and limitations of compression liquefaction and metal hydride adsorption methods of hydrogen storage, which they maintain would position hydrogen as a major energy carrier towards the reduction of greenhouse gas emissions and the development of stronger and more diverse energy systems.[3] It is possible to make the production of high-purity hydrogen sustainable via electrochemical water splitting, provided that the electricity is renewable. The technique makes it scalable, leaves no toxic waste, and is friendly to the environment. The rate of inefficiency. The splitting of water is considerably limited due to the slow rate of oxygen evolution reaction (OER) kinetics, which entail hectic multi-electron transfer mechanics and large energy requirements. Not only does the OER have dozens (or more) oxygen-binding transition states to traverse, to bind, and to split, but this is a huge bottleneck by comparison to the HER, where much

simpler one-electron transfer occurs. Future progress of hydrogen energy technologies is based on the development of inexpensive electrocatalysts with a high level of activity and stability of the OER.[4]

Noble metal oxides, e.g., ruthenium dioxide (RuO2) and iridium dioxide (IrO2), are mentioned as amongst the most promising OER catalysts, in which their breathtaking intrinsic activity tends to be described as a yardstick.[5] As Qian et al demonstrated, a combination of high-entropy RuO2 catalyst could not only achieve an extremely high intrinsic OER activity but also remarkably long-term stability even at the acidic condition because of a dual-site oxide pathway that overcomes the shortcomings of conventional adsorbate evolvement pathways. [6] It is, however, limited in wide usage in comparison with other elements due to its high cost, low abundance, and poor sustained characteristics under a harsh electrochemical environment. Consequently, more interest has emerged in finding alternative sources of transition metal-based catalysts that come from the earth.[7] A vast range of potential transition metal compounds of oxides, hydroxides, sulphides, nitrides, phosphides, and chalcogenides have all been demonstrated with good OER activity, and this can largely be ascribed to the tunable redox behaviour and the possibility of tuning crystal chemistry. The transition metal oxides, in general, and mainly due to abundance, multivalent redox states, high charge carrier mobility, and large specific surface area, are favoured, as well. The latter causes the enhanced electrocatalytic activity and the general tendency of the activity NiO > CoO > FeO > MnO, which is identified owing to the alterations of the electronic structure and adsorption properties of the intermediate. This is unlike other transition metal oxides, which exhibit irreversible redox reaction in addition to low density of oxygen vacancies and O formation, which is attributed to its much reversible Ce4+/Ce3+ redox couple, low density of oxygen vacancies, and strong O storage capacity that makes it desirable both electronically and ionically conductive. CeO_2 possesses this property, and this is the factor that predetermines the prospect of using it as a platform for OER electrocatalysis.[8] The formation of a hydroxide-terminated CeO_2 interface using NiFeCr overlayer on Cu@CeO_2 nanotubes was studied by Xia et al., especially because this interface effectively tailored the electron and oxygen conduction routes and produced high catalytic activity with outstanding long-term electrochemical stability in alkaline conditions due to OER.[9] Moreover, the uses of catalysis are not only limited to that of catalysis but also extend to the fields of solid oxide fuel cell, gas sensing, and photocatalysis, hence, further augmenting the technological importance.

Elemental doping is an efficient tool and has been developed in the past few years to engineer structural, electronic, and catalytic properties of nanostructured materials. By doping a host lattice with dopant species, researchers are able to modify properties of the material that are vital to its performance, namely, band structure, surface chemistry, and density of defects. In the case of CeO_2, several dopants such as Fe, Mn, Eu, Gd, and Zr were utilized to improve the OER activity of this material. It has been demonstrated that iron doping will bring disorder and reduce the amount of overpotential needed to perform OER, and Mo- or Co-doped CeO_2 composite has also shown better catalytic performances at other electrochemical systems. Among others, zirconium is of special interest since it comprises a structurally and chemically compatible material with oxides containing cerium. The close proximity in ionic radius and electrical charge (Zr has an ionic state of +4 and Ce has an ionic state of +4) gives the possibility to easily substitute the ions in the fluorite lattice, which is favourable to the formation of vacancies due to vacant oxygen sites in the lattice and distortion. The changes give way to redox adaptivity to produce ce4+/ce3+ as well as to charge transport and movement of oxygen ions. Zr doping can also induce porous nanostructure growth due to high surface area and enhanced conductivity, and thus can significantly expand the active sites that can be used to perform OER. Moreover, due to the existence of the surface hydroxyl groups together with oxygen-depleted areas produced by the addition of the Zr, the optimized catalytic kinetics and the adsorption of the reaction intermediates are significantly improved. In particular, the traditional trial-and-error methods of catalyst optimisation can be quite time-consuming and ineffective, especially in a system with many variables (dopant concentration, synthesis conditions, and compositional complexity). In this regard, machine learning (ML) can provide a revolutionary application to speed up catalyst discovery and optimization. ML models are able to analyse very large experimental data, make non-

obvious correlations, and make predictions on catalyst performances and overpotential ones with high accuracy. They prove helpful, especially in scenarios where an individual would be interested in studying the effect of the different metal dopants on the large composition landscape.

In the present study, optimisation is done to synthesise and work on the activity of Zr-doped CeO_2 electrocatalysts towards OER based on neural networks. The CeO_2 samples, which are synthesised in various coordinates of Zr (1-5) using hydrothermal methods, have been further drop-cast on a nickel foam of porous structure. A full characterisation set-up with the utilisation of SEM, TEM, HRTEM, XRD, FTIR, and UVV spectroscopy is carried out on morphology, structure, and optical properties. The values of important parameters such as dopant concentration, drying time, and deposition density were then optimised with the help of ML models to achieve the optimal performance of OER. The 3 wt% Zr-CeO_2 /NF catalyst yielded the best electrocatalytic activity in that the studied compositions exhibited low overpotential, low Tafel slope, and current density. The improvement is explained by the synergistic communication between the doped Zr, the oxygen disorders, and the animated group of Ce3+/Ce4+ redeployment that led to increased charge coverage and better capacity to absorb oxygen.

2. Experimental procedures

2.1 Materials Synthesis

Cerium oxide (CeO_2) nanostructure, as well as its Zr-doped corresponding specimen Zr-CeO_2 nanostructure, was achieved through an easy hydrothermal treatment. Normally, in synthesis, the appropriate stoichiometric quantities of cerium nitrate hexahydrate [Ce(NO3)3.6H2O] and zirconium nitrate [Zr(NO3)4-5H2O] were dissolved in deionized water to obtain Zr-doping levels of 0, 1, 3, 5, 7, and 10 molar ratios in relation to Ce. By adding aqueous ammonia, the PH of the solutions at which they were buffered was pushed to around 9, and then they were vigorously stirred to create the nucleation. The solution was thereafter poured into a stainless steel autoclave (lined with Teflon) and kept at a constant temperature of 180 °C, and left to stand for a period of 12 h. The obtained precipitate was cooled and washed repeatedly with ethanol and water (deionized water), which was then dried at 60 °C and later crushed to a fine powder.

2.2 Electrode Preparation

In order to prepare the working electrode, 1 mg of powdered Zr-CeO_2 was processed and dispersed in a solution that had isopropanol, Nafion (5 wt%), and deionized water in a 4:1:5 volume ratio. In order to encapsulate the suspension completely, a 30-minute ultrasonication was performed. Subsequently, 10 μL of the formed ink was drop-casted on a pre-cleaned nickel foam (NF) substrate (area of 1cm2) and dried at ambient temperature just before providing it with a uniform catalyst layer. With the machine learning programmed, the dryer time and the loading quantity were matched against each other poorly methodically.

2.3 Material Characterization

SEM, TEM, and HRTEM were used to describe them in terms of their morphology and microstructure. The crystalline phases were confirmed through XRD, and the surface functional groups were determined with the help of FTIR. UV-Vis diffuse reflectance Spectroscopy (UV-Vis DRS) optical properties and Bandgap energies were used to describe them. X-ray photoelectron spectroscopy (XPS) was employed to remove the information of chemical surfaces, i.e., the valence states and chemical constituents of the valence level of the Ce3+/Ce4+ and the content of the Zr4+.

2.4 Electrochemical Measurements

The electrochemical oxygen evolution reaction (OER) performance was assessed by means of the individual instrumental methods using a standard three-electrode cell with the electrolyte containing

a 1.0 M KOH aqueous solution. The working electrode was the Zr-CeO_2/NP, the reference was a Saturated calomel electrode (SCE), and the counter was a platinum wire. All these potentials were charged to the reversible hydrogen electrode (RHE) scale, and the linear sweep voltammetry (LSV) was measured at 5 mV/s. Frequency of refractive index. The behavior shown by the electrochemical impedance spectroscopy (EIS) was obtained in a frequency range between 100 kHz and 0.01 Hz. Electrochemically active surface area (ECSA) teaching was carried out with the help of calculated double-layer capacitance (Cdl) values using cyclic voltammetry (CV) data, where the scan rate is varied.

2.5 Machine Learning Optimization

Eight regression models are used, namely Gradient Boosting Regression (GBR), AdaBoost, Extra Trees Regressor, Decision Tree, Lasso, Ridge, K-Nearest Neighbors (KNN), and XGBoost (XGBR), that predict the overpotential values by using experimental input data parameters of Zr concentration, amount of catalyst loading, and drying time. These data are already segmented into 80 percent training data and 20 percent testing data. Hyperparameter optimization has been performed with the help of the grid search in a 10-fold cross-validation. The model with the highest R^2 score and also root-mean-square error (RMSE) was utilized as the best performing one. Ranking the feature importance was derived to be able to select the most powerful features, and the best result in an experiment was achieved and yet proven.

3. Results and Discussion

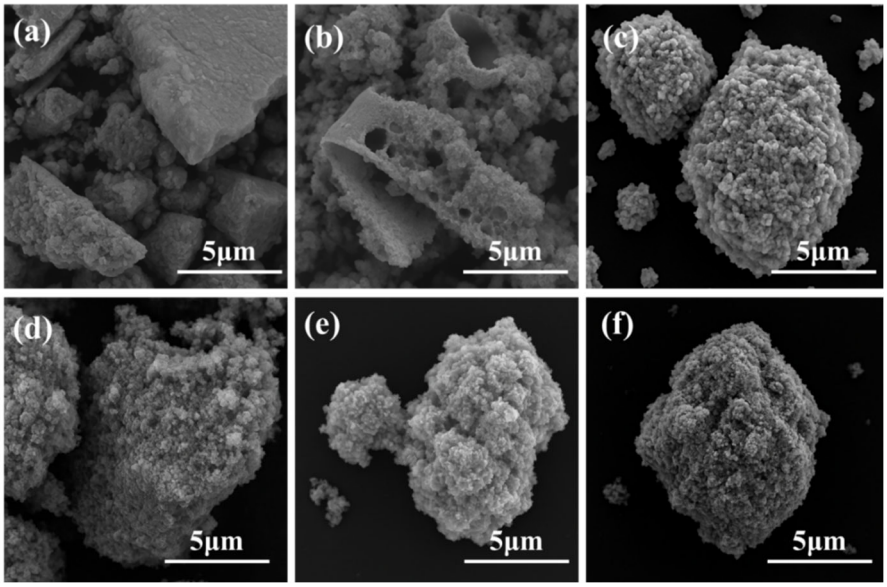

Fig.1 Morphological Evolution of CeO_2 upon Zr Doping. (a) Pure CeO_2, (b) 1%Zr-doped, (c) 2%Zr-doped, (d) 3%Zr-doped, (e) 4%Zr-doped, (f) 5%Zr-doped.

Figure 1 shows the morphological variation of CeO_2 particles with a change in Zr-doping level as observed by field-emission scanning electron microscopy (FESEM). The undoped CeO2 (Figure 1a) features irregularly shaped aggregates constituted of fully packed primary crystallites, with a relatively smooth surface and a small amount of mesoporosity. With the addition of 1 mol/Zr of Zr (Figure 1b), the particle structure is more granular and with visible pore channels and cavity holes, demonstrating that, at low concentration incorporation, Zr disrupts crystal growth kinetics and stimulates defect-mediated surface etching. A higher doping of 2 mol.% results in looser, more spherical secondary particles with a higher interparticle void fraction (Figure 1c), which potentially is more advantageous to electrolyte penetration during electrocatalysis. The material is hierarchical in structure and resembles coral-like structures on the nanoscale at 3 mol% Zr (see Figure 1d), with a large specific surface area and potentially increased catalytically active site density. This micro/nanostructure may be attributed to a synergistic equilibrium between the nucleation rate and

growth rate at optimal dopant concentration that allows uniform distribution of defects. An additional increase of Zr up to 4 mol% (Figure 1e) results in tighter spherical aggregates, but with preserved surface roughness and porosity, indicating only partial fusion of nanoparticles. The doping level at which this morphological change occurred was the greatest treated (5 mol%) in Figure 1f, where the most prominent feature was the more compact, almost monolithic, spherical shape with fewer surface irregularities, which suggests the migration of grain boundaries and the grain boundary sintering process at the dopant-induced, post-synthesis thermal treatment. Altogether, the gradual morphological evolution of irregular aggregates into well-ordered microspheres, as well as the changes in the surface texture and porosity, prove that the effect of Zr doping has a strong impact on CeO_2 crystal development pathways. Intermediate concentrations Doping (2-3 mol%) seem to yield an optimized microstructure in terms of a combination of high surface area and mechanical stability, potentially leading to better electrochemical performance in the Oxygen evolution reaction (OER).

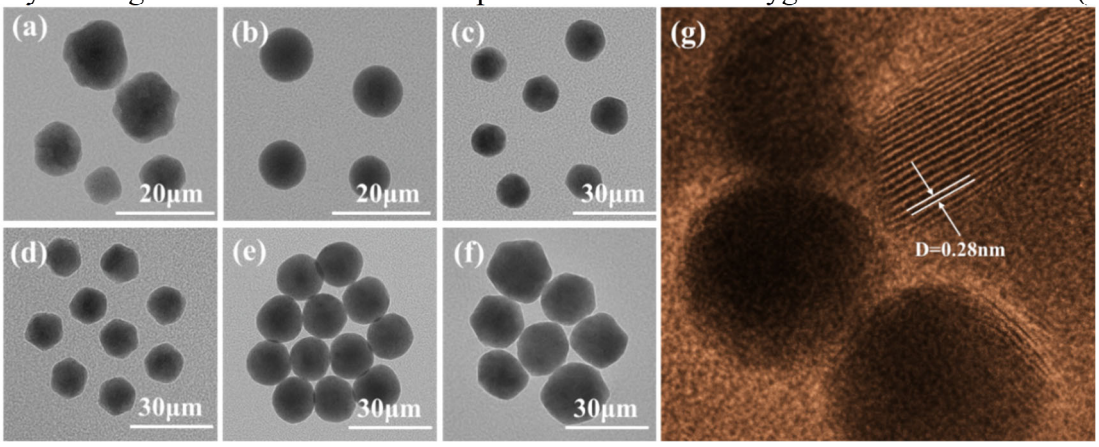

Fig.2 TEM and HR-TEM Analysis of Zr-Doped CeO_2 Nanostructures.

Transmission electron microscopy (TEM) and high-resolution TEM (HR-TEM) mapping of CeO_2 and Zr-doped CeO_2 nanostructures of different Zr content are displayed in Figure 2. The as-grown undoped CeO2 particles (Figure 2a) also exhibit irregular morphologies of polyhedra with a touch of rough edges; this represents anisotropic crystal growth. With 1 mol% Zr doping (Figure 2b), particles exhibit a more uniform morphology with well-defined quasi-spherical shapes and smoother surfaces, indicating that low levels of Zr doping stabilize certain crystal facets and inhibit any uncontrolled growth facets. With further addition of Zr (to 2 mol% Zr in Figure 2c), nanostructures are in almost perfect monodispersity and polysperse, implying well-controlled nucleation of the synthesis process. The self-organization of Zr particles at 3 mol% (Figure 2d) shows smaller diameters and more pronounced contrast that may be attributed to better crystallinity and an elevated electron density caused by the presence of Zr dopants. The packed nature of the spherical particles in the 4 mol% Zr-doped sample (Figure 2e) results in a small interparticle distance, which potentially facilitates the formation of electron transport pathways, but is likely to limit the available surface area. With the maximum doping concentration of 5 mol% (Figure 2f), the particles tend to be more faceted and have more close-packed shapes, revealing the growth kinetics changes due to doping that will promote thermodynamically stable shapes of bases. And lattice fringes isolated in the HR-TEM image (Figure 2g) indicate an interplanar spacing of 0.28 nm (cubic fluorite structure of CeO_2, (200) plane). High crystallinity of the particles in all levels of doping is confirmed by the sharp lattice contrast. The fact that Zr incorporation did not induce substantial lattice distortion is that effective substitution of the Ce4+ lattice sites by Zr 4+ occurs without forming new phases, as indicated by XRD data. Altogether, the TEM and HR-TEM observations confirm that ceasing doping of Zr allows us to precisely manipulate CeO_2 nanoparticle morphology and crystallinity that would play an important role in determining electrochemical performance in oxygen evolution reaction (OER) catalysis.

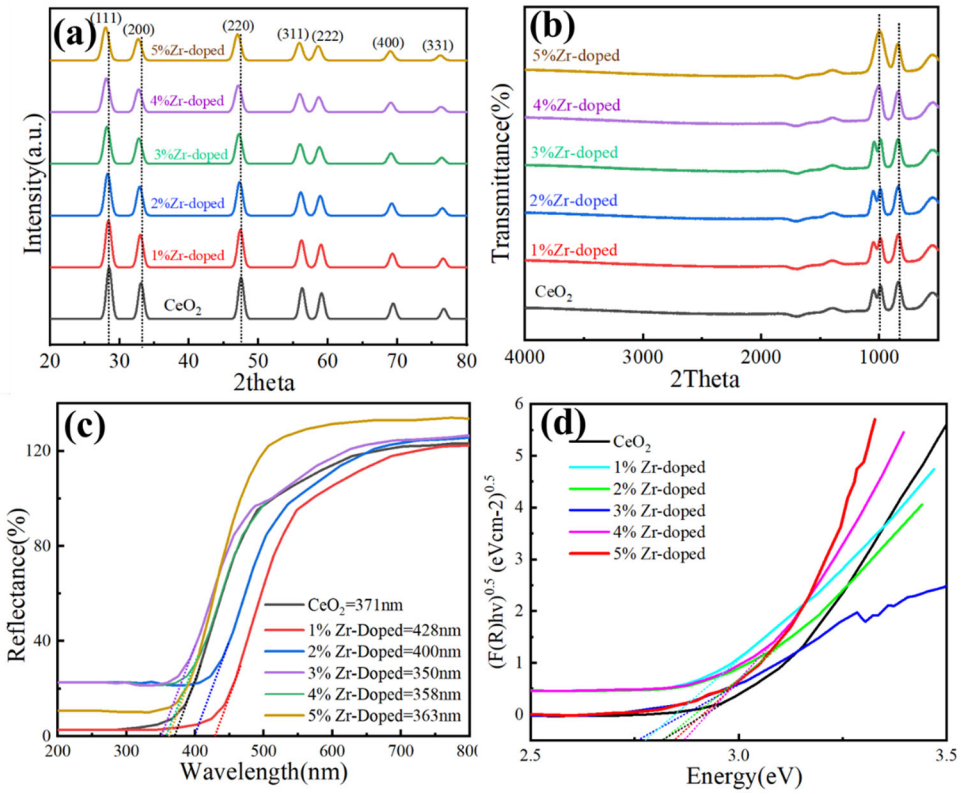

Fig. 3 XRD patterns (A), FTIR spectra (B), UV-reflectance spectra, and optical band energy interpretation spectra of (C, D) CeO_2, 3% Zrdoped CeO_2, and 5% Zr- CeO_2.

Figure 3 illustrates the changes in structure, vibrational, and optical properties of CeO_2 on Zr doping. X-ray diffraction (XRD) spectra (Figure 3A) of pure and Zr-doped CeO_2 exhibit sharp peaks attributed to the 2 theta indicating (111), (200), (220), (311), (222), (400), (331) and (420) planes of a cubic fluorite structure (JCPDS 34-0394). The lack of secondary phases proves the incorporation of Zr4+ in the lattice of CeO_2 without the formation of segregated zirconia. Interestingly, a minor monotonic change in peak positions during doping implies lattice shrinkage because of the lower ionic radius of Zr4+ (0.72 Å) than that of Ce4+ (0.87 Å), which results in strain and a possible enhancement of the oxygen vacancy concentration. FTIR spectra (Figure 3B) show typical Ce-O stretching modes at 500-600 cm-1 in all samples, which develop slight changes in intensity with doping, indicating alteration of local bonding sites. Other weak bands in doped samples are ascribed to modes associated with defects, in agreement with the lattice distortion amplified. UV-Vis diffuse reflectance spectra (Fig. 3C) exhibit redshifts in absorption edges between Zr-doped samples and pure CeO_2, and estimated absorption onsets of 382 nm (pure), 358 nm (3% Zr), and 368 nm (5% Zr). Comparable Tauc plots (Figure 3D) reveal narrower optical bandgap electrons of 2.91 eV (in pure CeO_2) to 2.76 eV (3% Zr) and 2.85 eV (5% Zr). This bandgap constriction is attributed to defect levels caused by doping with Zr, allowing increased electronic transport and, additionally, an improved charge transfer in the course of electrocatalytic reactions. These findings altogether can attest to the fact that controlled Zr insertion into CeO_2 keeps the fluorite structure with minor lattice distortions, changes in vibrational properties, and reduces the bandgap. The same structural and electronic modifications are predicted to have synergistic effects on the efficient oxygen evolution reaction (OER) performance due to the optimization of the trade-off between electrical conductivity and the active site accessibility.

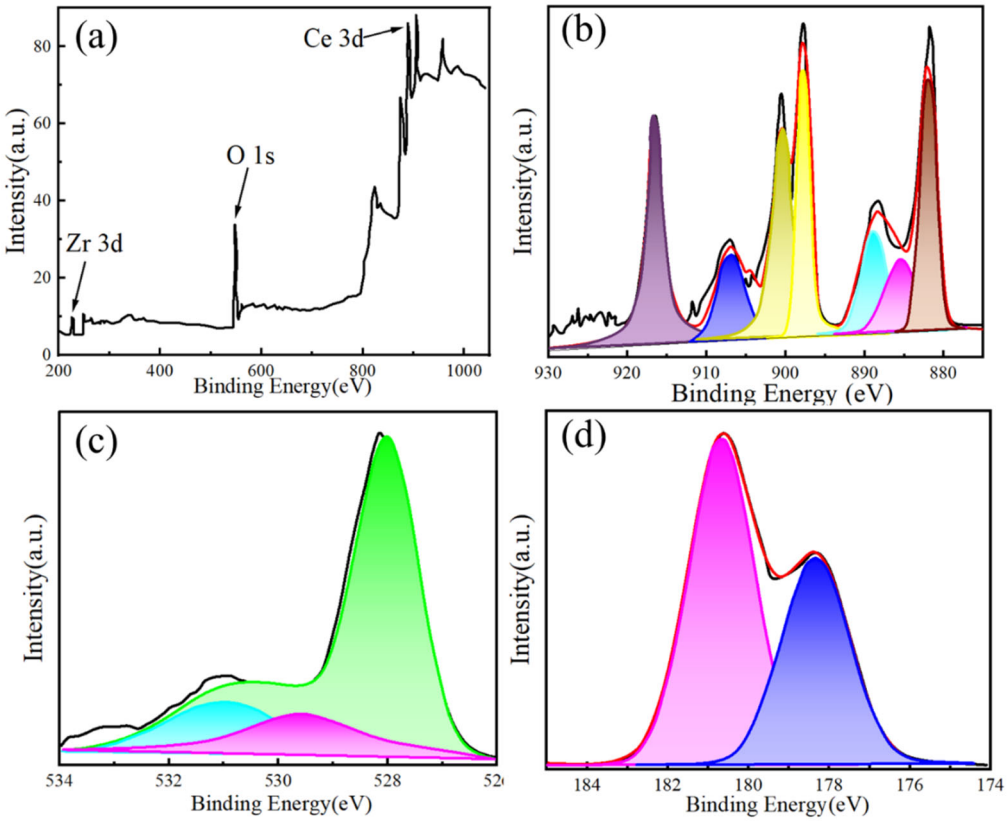

Fig. 4 XPS spectrum of 3% Zr-doped CeO_2 (a) and survey spectrum of (b) Ce, (c) Zr, and (d) O.

The X-ray photoelectron spectroscopy (XPS) data of 3 mol% Zr-doped CeO_2 are shown in Figure 4, where information is obtained about elemental composition and oxidation states, as well as the chemistry on the surface. The wide-scan survey spectrum (Figure 4A) shows clear and characteristic Ce 3d, Zr 3d, and O 1s peaks, being irrefutable evidence of successful incorporation of Zr without any distinctive sign of an impurity phase. The Ce 3d spectrum (Figure 4B) is repeated with several spin-orbit doublets representing both Ce4+ and Ce3+ forms. The highest-intensity peaks at the highest binding energies are attributed to the Ce 4 + final states (v, v ', v '', u, u ', u '''), implying that oxygen vacancies and mixed-valence states exist. Additional lower-intensity peaks are attributed to the Ce 3 + (v 0, u 0). The relative Ce3+ content indicates that the doping with Zr is effective in the partial reduction of Ce4+, thus being favorable to the concentration of the defects useful to catalytic reactions. The XPS O 1s spectrum (Figure 4C) could be deconvolved into three main parts comprising lattice oxygen peak (~529.2 eV), oxygen vacancy component (~530.5 eV), and the surface hydroxyl/adsorbed oxygen species (~531.8 eV). The high intensity of the vacancy-related peak in the doped sample confirms the enrichment of Ce3+ in the Ce 3d spectrum, which supports the hypothesis that the incorporation of Zr promotes the formation of vacancy by charge compensation. The Zr 3d signal (Figure 4D) reveals good resolution peaks at ~182.3 eV (Zr 3d 5/ 2) and ~184.7 eV (Zr 3d 3/ 2) characteristic of Zr4+ in an oxide lattice. Lack of lower valence states of Zr can be adduced as evidence that fully oxidized Zr is substitutionally inserted into the CeO_2 lattice and any phase of metallic or sub-oxide composition is eliminated.

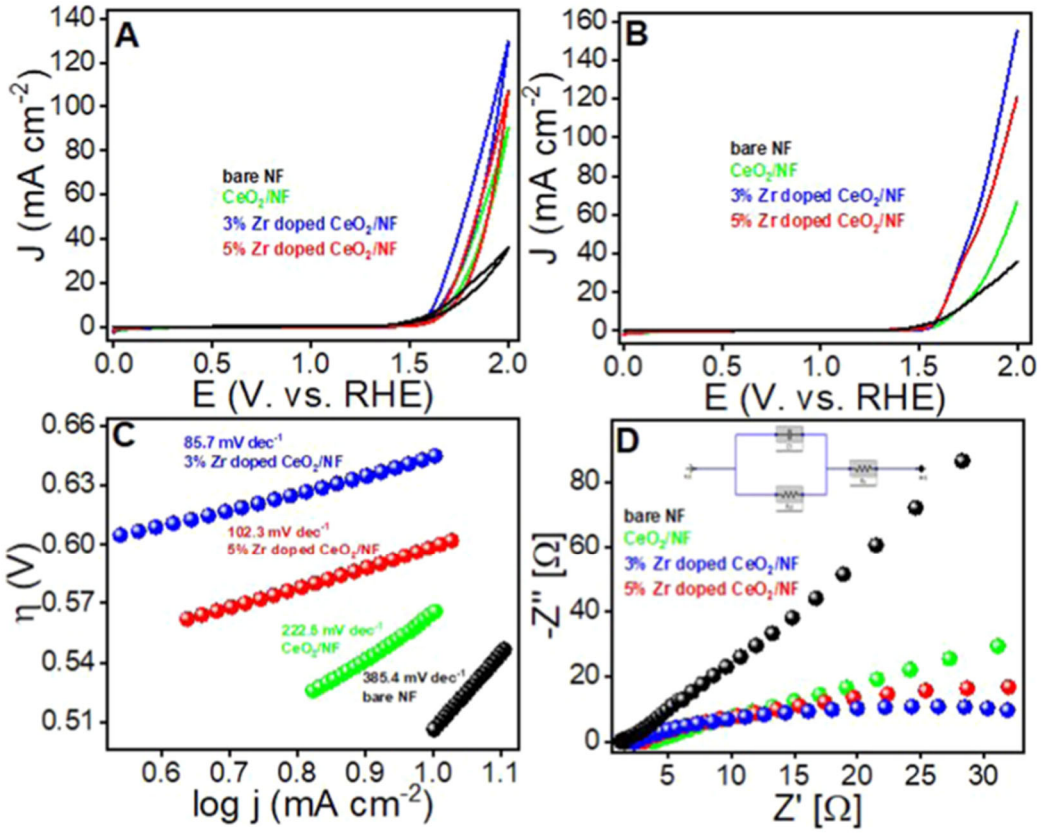

Fig. 5 Bare NF, CeO_2/NF, 3% Zr-doped CeO_2/NF, and 5% Zr-CeO_2/NF Electrocatalysis data: (A) CV and (B) LSV. Lateral Tafel plot of bare NF, CeO,/NF, 3% Zr-doped CeO,/NF, and 5% Zr-CeO,/NF constrained using the LSV curve. Nyquist plot containing Randle circuit (D), which includes the charge transfer and solution resistance at the interface between the electrode and electrolyte.

Figure 5 demonstrates the overall electrochemical examination of naked NF, CeO_2/NF, and Zr 2/CeO_2/NF electrodes, showing the effect of adding Zr on oxygen evolution reaction (OER) performance. It is apparent in panel A (CV) and B (LSV) that Zr doping substantially lowers the starting potential and enhances current density in comparison to undoped CeO_2 and bare NF, which denotes improved intrinsic activity. It is interesting, however, to note that the 3% Zr-CeO_2/NF electrode demonstrates maximal current density at similar potentials. Panel C shows the corresponding Tafel plots obtained using the LSV data, which gives some information on reaction kinetics. The much smaller Tafel slope of CeO_2 /NF (22.8 mV dec 1) compared with bare NF (385.4 mV dec 1) indicates faster charge transfer kinetics, but Zr doping alters the slope according to the dopant concentration, which again indicates an altered rate-determining step. In Panel D, there are Nyquist plots using the electrochemical impedance spectroscopy (EIS), and fit Randle's circuit models. The diminution of semicircle diameter 2 in Zr-doped electrodes and especially 3% Zr-CeO_2/NF reflects significantly reduced charge transfer resistance, which is advantageous to rapid electron transport across the electrode-electrolyte interface.

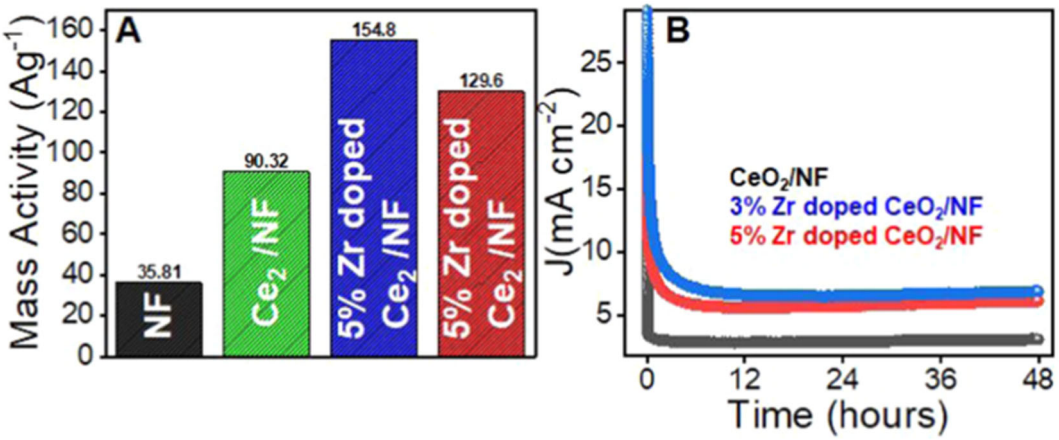

Fig. 6 Mass activity of fabricated materials, i.e.,CeO_2/NF, 3% Zr-doped CeO_2/NF, and 5% Zr-CeO_2/NF (A). Chronoamperometric experiments to approximate the stability and durability.

The corresponding Figure 6 gives essential data both on the inherent catalytic activity and the long-run operational stability of fabricated CeO_2/NF/ and Zr-doped CeO_2/NF electrodes. Panel A draws a comparative picture of the mass action of bare NF, undoped CeO_2 /NF, and two Zr doping derivations. Tremendous increase in mass activity is noted on Zr incorporation, where 5% Zr-CeO_2/NF shows the maximum value (154.8 A g 1), followed by 5% Zr-CeO_2/NF (post stability test) at 129.6 A g 1, and undoped CeO_2/NF records 90.32 A g 1. Bare NF, on the other hand, shows significantly deactivated activity (35.81 A g -1). These values demonstrate that the Zr doping leads to the rise of the accessible amount of active sites per unit mass successfully, probably because of the provision of defects and enhanced electronic conductivity. On panel B are shown chronoamperometric results during the 2 days of continuous operation at constant potential. The current density of all electrodes declines rapidly at the first stage due to the processes of restructuring on the surface and wetting with the electrolyte, and subsequently reaches the steady-state stage. The Zr 3% and 5% CeO_2/NF/NF electrodes are performing at much higher current densities than the undoped CeO_2/NF during the test, as evidence of their better sustainability under prolonged electrochemical stress. Notably, the Zr-doping delivers a negligible performance degradation in the samples, demonstrating the stability of their structural integrity and the stability of catalytic interfaces, which is pivotal towards practical use.

This paper was used to explore the analysis of the effect of ML in predicting overpotential on diverse compositions of CeO_2/NF and 1, 2, 3, 4, 5 % Zr-doped CeO_2/NF, with implementation of different regression models (LR, DTR, Lass R, RFR, GBR, KNNR, ENR, and XGBR) on the experimental dataset (ED). Multiple regression models were used to construct a quantitative relationship between a dependent variable (Overpotential) and one or more independent variables (zirconium percentage (%), material deposited (mg) and drying time (min) of Ce(NO3)3·6H2O and Zr(NO3)4 in the fabricated CeO_2/NF, 1, 2, 3, 4, 5 %Zr doped CeO_2/NF. The process of the dataset assessment that was carried out by the regression model focuses mainly on dividing the available information into three different subsets, namely the training set, the validation set, and the test/prediction set. First, the training dataset is used to fit the regression models and then validated on the validation and the test datasets. The accuracy and quality of prediction are thoroughly examined with the error metrics being the root-mean-square error (RMSE) and the corrected R-square (R2).

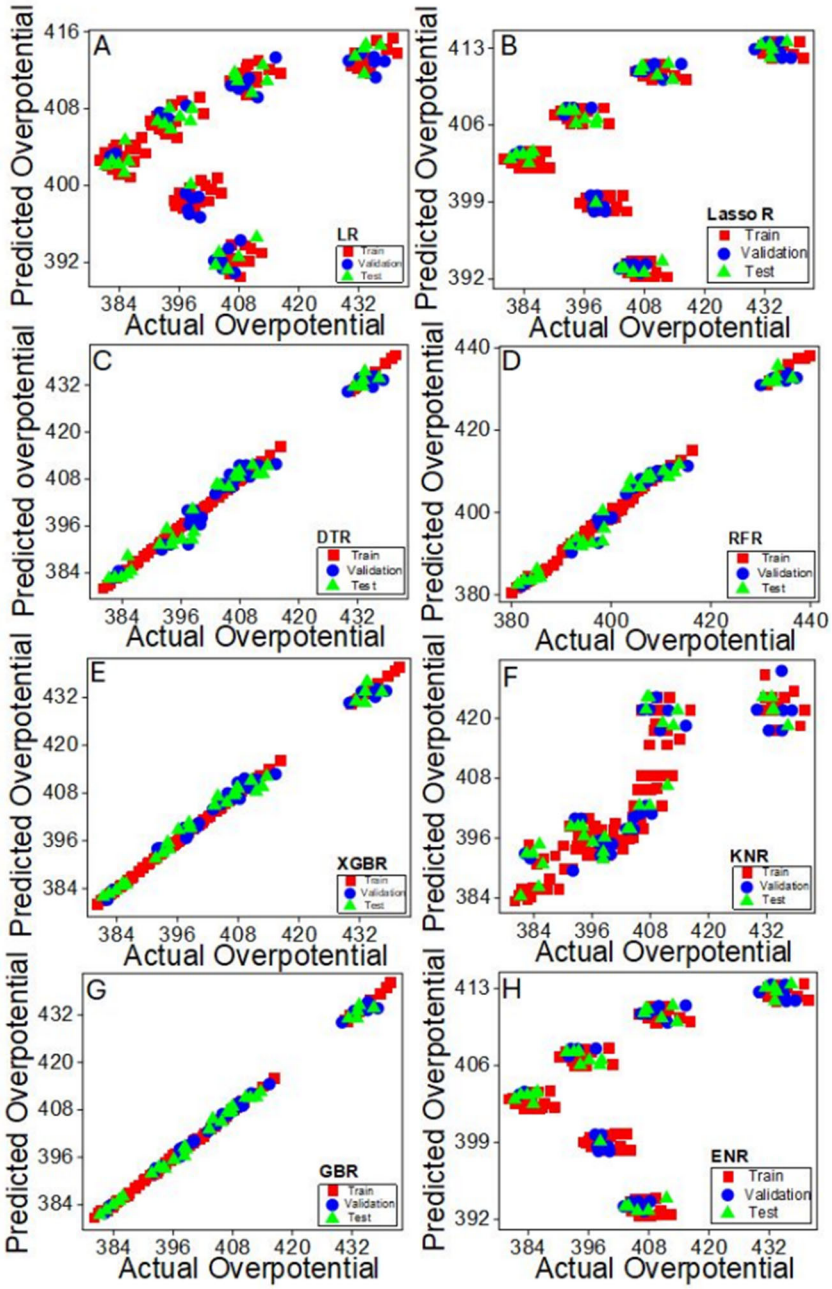

Fig.7 Comparative examination, prediction of overpotential response, using eight different regression models.

To hasten the optimization of Zr-doped CeO_2 electrocatalysts for the oxygen evolution reaction (OER), eight different regression models were generated and tested on how well they predicted the overpotential using experimental variables, such as the Zr doping amount, catalyst loading, and drying time. Figure 8 contrasts the mean value of the predicted versus actual overpotential in each model, and data points reflect training, validation, and testing subsets. The linear regression (LR) and elastic net regression (ENR) models (Figures 8A and S1H) show a rather low predictive accuracy as data points are widely scattered and significantly deviate around the parity line. Correspondingly, the lasso regression (Lasso R) model (Figure 8B) is also underperforming, which demonstrates that strictly linear methodologies are not effective at characterizing a non-linear dependence between synthesis parameters and electrochemical performance. Instead, tree-based ensemblers, i.e., decision tree regression (DTR), random forest regression (RFR), extreme gradient boosting regression (XGBR), and gradient boosting regression (GBR) (Figures 8C-8G) exhibit outstanding predictive performance, with an R 2 close to unity and a root-mean-square error (RMSE) close to zero in both training and test datasets. Notably, GBR and XGBR show a near-perfect ratio of estimated and real

values of overpotential from each data partition, and therefore, it is more up to the mark in small non-linear datasets with multi-variable interaction studies. The k-nearest neighbors regression (KNR) model (Figure 8F) is positioned halfway between the most accurate and least accurate models, with very strong overfitting in the training range and only slightly less so in the test set. The high quality of gradient-boosted and ensemble trees publications supports the surmise that the OER overpotential of Zr-CeO_2 catalysts is highly influenced by complex synergistic interactions among structural defects, electronic conductivity, and surface active site density - relationships that cannot be described in full extent by such linear models.

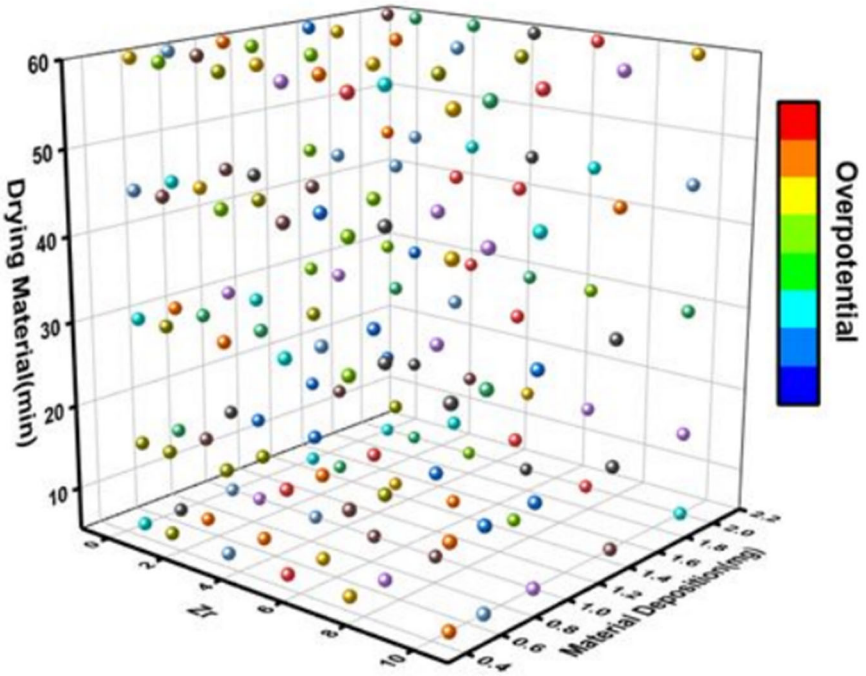

Fig. 8 Details how the potential overpotential behaviour of the DTR model is affected by a range of experimental parameters.

Figure 8 shows a three-dimensional scatter plot created with the help of the Decision Tree Regression (DTR) model in which the predicted overpotential is plotted against three most important experimental parameters, i.e., the Zr doping level on the x-axis, the amount of catalyst deposited onto the y-axis, and the time during drying on the z-axis. A color map indicates the value of the overpotential, with the lowest values (dark blue) and highest values (dark red), allowing an immediate visual recognition of those areas of parameters that are optimal. It is clear that there are significant non-linear relations and interdependences of synthesis variables, as shown by the distribution of the points. The regions of low overpotential-marked by blue and green spheres-are mainly concentrated around medium concentration of Zr doping (3-5 percent), and medium loading (~1.0 mg) of the catalyst, as well as medium duration time of drying (30-45 min). It is probable that such combinations of parameters would balance various catalytic enhancement processes, such as optimal surface morphology, optimal adhesion of the catalyst layer to the nickel foam substrate, and optimal oxygen vacancy formation. Similarly, extreme values in a single parameter, including excessive overdoping of Zr, untenable drying times, or heavy loading of the catalyst, are noted to be accompanied by large overpotentials (yellow to red spheres). These deviations can lead to suboptimal structural or electronic properties, either by having insufficient active sites, or by closing off access to the electrolyte by catalyst films that are too dense. Through neural network interpretability, this visualization takes advantage of the DTR model to partition the multi-dimensional design parameter space using the non-linear optimization landscape unique to catalyst design. Notably, the 3D mapping allows identifying sweet spots on a narrow parameter range where the synergy of parameters can produce a small overpotential. Such a strategy decreases the level of trial and error experiments that are labor-heavy and also shows the helpfulness of machine learning in the direction of electrocatalyst synthesis, oriented towards high-performance designs with a minimum number of experimental repetitions.

Table 1 represents the RMSE and %R2 of each ML algorithm on the training, validation, and test datasets.

Model	Train RMSE	Validation RMSE	Test RMSE	R2 Score
Linear Regression	14.05	13.53	14.28	0.21
Lasso Regression	14.09	13.45	14.55	0.18
Elastic Net Regression	14.09	13.46	14.54	0.18
Decision Tree Regression	0.00	2.34	2.33	0.98
Random Forest Regression	0.72	1.89	2.16	0.98
Gradient Boosting Regression	0.32	0.89	0.98	1.00
K-nearest neighbor Regression	7.08	9.14	8.71	0.71
XGBoost Regression	0.01	1.57	1.61	0.99

4. Conclusion

Zr-doped CeO_2 nanostructures were successfully prepared and systematically tested as oxygen evolution reaction (OER) electrocatalysts, including optimizing the parameters used with the help of machine learning (ML). Extensive structural and electrochemical investigations showed that moderate Zr substitution, especially 3 mol%, is indeed a powerful method of controlling the CeO_2 lattice, forming oxygen vacancies, promoting Ce3+/Ce4+ flexible redox, and fine-tuning surface morphology. Such synergistic effects lead to a much smaller overpotential (UR = 319 mV at 10 mA cm-2), a lower Tafel slope (Tafel = 85.7 mV dec-1), and outstandingly good long-term stability that remains at 84 percent of the initial current density after 48 h of continuous working. Moreover, the ML models used have allowed significant predictive analyses on dopant-concentration, catalyst-loading, and processing-conditions interactions. The two most predictive models of the eight tested models were gradient boosting regression (GBR) and extreme gradient boosting regression (XGBR), which emphasize the potential of these as fast and effective means of catalyst discovery. Experimental data combined with ML-based optimization also reduced trial-and-error synthesis, as well as could be used to optimize the synthesis conditions, showing some of the best sweet spots in the parameters of synthesis, thus taking a step forward to the data-driven catalyst design. In general, this paper shows that doping with Zr is quite a viable approach toward boosting the OER electrocatalytic performance of CeO_2, whereas the ML-based optimization scheme provides a way of speeding up the design of high-performance non-noble metal electrocatalysts in general. The extension to multi-element doping, more complicated synthesis pathways, or assembly into complete water-splitting systems would be studied in future research and thus open the way to cost-effective and sustainable technologies of hydrogen production.

References

[1] Scheffmn, J., Modelling environmental conflicts and international stability. 1996.

[2] Lototskyy, M. and V. Linkov, Thermally driven hydrogen compression using metal hydrides. International Journal of Energy Research, 2022. 46(15): p. 22049-22069.

[3] .Hassan, Q., et al., Hydrogen as an energy carrier: properties, storage methods, challenges, and future implications. Environment Systems and Decisions, 2024. 44(2): p. 327-350.

[4] Liu, Y., et al., Cobalt-based Co3Mo3N/Co4N/Co metallic heterostructure as a highly active electrocatalyst for alkaline overall water splitting. Angewandte Chemie, 2024. 136(14): p. e202319239.

[5] Bai, J., et al., RuO2 Catalysts for Electrocatalytic Oxygen Evolution in Acidic Media: Mechanism, Activity Promotion Strategy and Research Progress. Molecules, 2024. 29(2): p. 537.

[6] Qian, F., et al., High-entropy RuO(2) catalyst with dual-site oxide path for durable acidic oxygen evolution reaction. Nat Commun, 2025. 16(1): p. 6894.

[7] Lunger, J., et al., Atom-by-atom design of metal oxide catalysts for the oxygen evolution reaction with machine learning. 2023.

[8] Peera, S.G. and S.W. Kim, Rare Earth Ce/CeO_2 Electrocatalysts: Role of High Electronic Spin State of Ce and Ce3+/Ce4+ Redox Couple on Oxygen Reduction Reaction. Nanomaterials, 2025. 15(8): p. 600.

[9] Xia, J., et al., Efficient optimization of electron/oxygen pathway by constructing ceria/hydroxide interface for highly active oxygen evolution reaction. Advanced Functional Materials, 2020. 30(9): p. 1908367.